Dissipative Quantum Feedback in Measurements Using a Parametrically Coupled Microcavity

Liu Qiu[1,*,‡] Guanhao Huang[1], Itay Shomroni[1,2], Jiahe Pan[1], Paul Seidler[3], and Tobias J. Kippenberg[1,†]

[1] *Institute of Physics, Swiss Federal Institute of Technology Lausanne (EPFL), Lausanne CH-1015, Switzerland*

[2] *Racah Institute of Physics, The Hebrew University of Jerusalem, Jerusalem 9190401, Israel*

[3] *IBM Quantum, IBM Research Europe, Zurich, Säumerstrasse 4, Rüschlikon CH-8803, Switzerland*

Micro- and nanoscale optical or microwave cavities are used in a wide range of classical applications and quantum science experiments, ranging from precision measurements, laser technologies to quantum control of mechanical motion. The dissipative photon loss via absorption, present to some extent in any optical cavity, is known to introduce thermo-optical effects and thereby impose fundamental limits on precision measurements. Here, we theoretically and experimentally reveal that such dissipative photon absorption can result in quantum feedback via in-loop field detection of the absorbed optical field, leading to the intracavity field fluctuations to be squashed or antisquashed. A closed-loop dissipative quantum feedback to the cavity field arises. Strikingly, this modifies the optical cavity susceptibility in coherent response measurements (capable of both increasing or decreasing the bare cavity linewidth) and causes excess noise and correlations in incoherent interferometric optomechanical measurements using a cavity, that is parametrically coupled to a mechanical oscillator. We experimentally observe such unanticipated dissipative dynamics in optomechanical spectroscopy of sideband-cooled optomechanical crystal cavitiess at both cryogenic temperature (approximately 8 K) and ambient conditions. The dissipative feedback introduces effective modifications to the optical cavity linewidth and the optomechanical scattering rate and gives rise to excess imprecision noise in the interferometric quantum measurement of mechanical motion. Such dissipative feedback differs fundamentally from a quantum nondemolition feedback, e.g., optical Kerr squeezing. The dissipative feedback itself always results in an antisqueezed out-of-loop optical field, while it can enhance the coexisting Kerr squeezing under certain conditions. Our result applies to cavity spectroscopy in both optical and superconducting microwave cavities, and equally applies to any dissipative feedback mechanism of different bandwidth inside the cavity. It has wide-ranging implications for future dissipation engineering, such as dissipation enhanced sideband cooling and Kerr squeezing, quantum frequency conversion, and nonreciprocity in photonic systems.

Dissipation is the hallmark of an open quantum system, which leads to undesired decoherence and hinders the observation of quantum phenomenon. The developments in nanofabrication over the last decades enable engineered low-loss optical microcavities for a wide range of novel

physics and applications in cavity based measurements or transduction [1–4], ranging from frequency metrology, to cavity quantum electrodynamics and cavity optomechanics. Dissipative absorption of photons is ubiquitous in optical cavities of different scales [5–8]. Such photon absorption manifests as a feedback mechanism to the optical cavity field, e.g., by changing cavity properties. Optical absorption is widely employed in photonic technologies [9–13], such as thermal tuning, optical switching, and sensing. The incoherent photon absorption has been shown theoretically and experimentally to limit precision measurements [14–18], such as in the gravitational wave detection [14], position measurements [19,20], and frequency metrology [18,21]. However, the influence of dissipative dynamics due to photon-absorption-induced feedback in the widely used microcavity spectroscopy still remains unexplored.

We show that a closed-loop dissipative quantum feedback arises in a microcavity due to photon absorption [22–24]. The optical absorption can be modeled by an in-loop detection of the absorbed photons, whose fluctuations can be squashed or antisquashed. The stochastic fluctuations in absorption lead to cavity frequency fluctuations, which results in a feedback loop to the cavity field [23–25]. The dissipative feedback gives rise to a modified optical cavity susceptibility, changing the optical transduction for the probing field and intracavity field. The optical cavity under such a condition is equivalently coupled to a dissipative reservoir, whose noise properties are different from the original vacuum noise, which causes excess noise in the out-of-loop measured optical field. The dissipative feedback introduces excess classical correlations in interferometric quantum measurement due to uncorrelated noise from the in-loop detection, an effect similar to laser noise [26–28].

More specifically, we report the observation of such dissipative dynamics in optomechanical spectroscopy of sideband cooled of 5-GHz mechanical breathing mode in optomechanical crystal cavities (OMCs) [29–34]. The optomechanical interaction via radiation pressure in a cavity has received significant interest over the last decade [4], enabling ground-state cooling [32,35–40], quantum correlations [41–48], and a variety of recently emerged applications, such as nonreciprocal devices [49–51], or quantum transducers [52–58]. Macroscopic quantum effects have been explored [46,47,59–67], including motional sideband asymmetry [31,46–48,68,69], mechanical entanglement [61,62], and squeezing [64–67]. However, most of these quantum optomechanical protocols are currently only feasible in very few optomechanical systems [37,38, 70–72], mainly due to the ubiquitous dissipative photon absorption. More specifically, we perform optomechanical spectroscopy with two OMCs of different optical absorption losses at cryogenic temperature (approximately 8 K) and under ambient conditions, respectively. Strikingly, we observe a modified and power-dependent optical cavity linewidth in the coherent cavity response, due to the dissipative feedback. At cryogenic temperature (approximately 8 K), an antisquashed in-loop absorbed optical field leads to an effective narrowing of the optical cavity linewidth, which may be exploited for enhanced sideband cooling and even normal-mode splitting [73–75]. Counterintuitively, the incoherent optomechanical scattering rate is equally modified due to the effective cavity linewidth, profoundly influencing interferometric mechanical quantum measurements. The dissipative feedback also results in *excess noise* in the quantum measurement of the mechanical motion in the balanced heterodyne detection, increasing the noise floor above the vacuum noise level.

We compare such dissipative dynamics to a quantum nondemolition (QND) feedback [22,76], e.g., optical Kerr

squeezing. The dissipative photon absorption itself always generates excess noise in the out-of-loop optical field, regardless of the fluctuations in the in-loop absorbed optical field [23–25]. We identify a regime where the dissipative absorption can even improve the coexisting Kerr squeezing, which can be attributed to the coherent dissipative dynamics, and is evaluated for a state-of-the-art Si_3N_4 microresonator [8].

I. THEORY

We first consider an optical cavity of resonant frequency ω_c, which is coupled to an input field $\hat{a}_{\mathrm{ex,in}} = (\bar{a}_{\mathrm{in}} + \delta a_{\mathrm{in}})e^{-i\omega_L t}$ of frequency ω_L at a rate of κ_{ex}. In the rotating frame of the pumping frequency ω_L, the dynamics of the intracavity field $\hat{a}$ can be described via a quantum Langevin equation, that includes the dissipative photon absorption,

$$\dot{\hat{a}} = \left[i\left(\Delta - \Delta_{\mathrm{th}}\right) - \frac{\kappa}{2} \right] \hat{a} + \sqrt{\kappa_{\mathrm{ex}}}\hat{a}_{\mathrm{ex,in}} + \sqrt{\kappa_s}\delta\hat{a}_{s,\mathrm{in}}$$
$$+ \sqrt{\kappa_a}\delta\hat{a}_{a,\mathrm{in}}, \tag{1}$$

with $\Delta = \omega_L - \omega_c$, and $\Delta_{\mathrm{th}} = g_{\mathrm{th}}\delta T$ being the cavity frequency shift via the optical-absorption-induced temperature δT and transduction coefficient g_{th}. The intrinsic cavity losses κ_0 in this treatment is separated into an absorption loss channel with rate κ_a (expressing the equivalent rate of absorbed photons, which lead to local heating of the cavity material, followed by a photo-thermal-induced cavity frequency shift) as well as a scattering loss channel with rate κ_s (which does not lead to a local heating of the cavity material). As a result of the presence of two dissipation channels, from the input-output relations for an open quantum system [77], the optical cavity is driven by input vacuum fluctuations $\delta\hat{a}_{a,\mathrm{in}}$ and $\delta\hat{a}_{s,\mathrm{in}}$ from both channels [cf. Eq. (1) right-hand side], with the total cavity loss being $\kappa = \kappa_{\mathrm{ex}} + \kappa_a + \kappa_s$. In the weak coupling regime, we can linearize the intracavity field $\hat{a}(t) = \bar{a}(t) + \delta\hat{a}(t)$, with $\bar{a}$ the mean field amplitude and $\delta\hat{a}$ the field fluctuation.

Crucially, we adopt a quantum treatment of the dissipative photon absorption, whose field amplitude can be obtained by

$$\hat{a}_{a,\mathrm{out}} = \delta\hat{a}_{a,\mathrm{in}} - \sqrt{\kappa_a}\hat{a}, \tag{2}$$

with the corresponding absorbed photon flux operator:

$$\hat{I}_a = \hat{a}^{\dagger}_{a,\mathrm{out}}\hat{a}_{a,\mathrm{out}}. \tag{3}$$

The absorption photon flux is composed of two terms, i.e., a dc term $\bar{I}_a = \kappa_a|\bar{a}|^2$, and a fluctuating term,

$$\delta\hat{I}_a = \kappa_a(\bar{a}\delta\hat{a}^{\dagger} + \bar{a}^*\delta\hat{a}) - \sqrt{\kappa_a}(\bar{a}^*\delta\hat{a}_{a,\mathrm{in}} + \delta\hat{a}^{\dagger}_{a,\mathrm{in}}\bar{a}). \tag{4}$$

The dynamics of the temperature change due to the optical absorption is given by $\delta\dot{T}(t) = -\gamma_{\mathrm{th}}\delta T(t) + g_a\hat{I}_a$, where

$g_a \hat{I}_a$ is the rate of the temperature change due to the optical absorption and γ_{th} is the thermal decay rate. The temperature fluctuation δT is treated classically, and becomes correlated to the quantum fluctuations of the in-loop photodetection. For simplicity, we assume a one-pole model of the thermal heating response. More details considering the geometric dependence are discussed in Appendix C. The quantum Langevin equations of the linearized optical field fluctuations can be obtained in the frequency domain,

$$\chi_{c,0}^{-1}(\Omega)\delta\hat{a} = \sigma_d(\Omega)\kappa_a(\delta\hat{a} + \delta\hat{a}^\dagger) + \sqrt{\kappa_a}\delta\hat{a}_d$$
$$+ \sqrt{\kappa_{\text{ex}}}\delta\hat{a}_{\text{ex,in}} + \sqrt{\kappa_s}\delta\hat{a}_{s,\text{in}}, \quad (5)$$

with the *intrinsic* optical susceptibility,

$$\chi_{c,0}(\Omega) = 1/[\kappa/2 - i(\Omega + \bar{\Delta})], \quad (6)$$

and $\bar{\Delta} = \Delta - g_a\kappa_a g_{\text{th}}\bar{n}_c/\gamma_{\text{th}}$, incorporating the additional static cavity frequency shift. The mean intracavity photon number is $\bar{n}_c = |\bar{a}|^2 = \kappa_{\text{ex}}|\bar{a}_{\text{in}}|^2/(\kappa^2/4 + \bar{\Delta}^2)$. We note that, the intracavity field is coupled to an effective dissipative reservoir,

$$\delta\hat{a}_d = \delta\hat{a}_{a,\text{in}} - \sigma_d(\Omega)\left(\delta\hat{a}_{a,\text{in}} + \delta\hat{a}_{a,\text{in}}^\dagger\right), \quad (7)$$

by coupling additionally to the amplitude quadrature $(\delta\hat{a}_{a,\text{in}} + \delta\hat{a}_{a,\text{in}}^\dagger)$ of the absorption field. Here we introduce a unitless photon-number-enhanced dissipation coefficient,

$$\sigma_d(\Omega) = \frac{g_a g_{\text{th}}}{\Omega + i\gamma_{\text{th}}}\bar{n}_c, \quad (8)$$

with $\sigma_d^*(-\Omega) = -\sigma_d(\Omega)$. The constant single-photon dissipation coefficient is given by $\sigma_0(\Omega) = \sigma_d(\Omega)/\bar{n}_c$.

Novel dynamics arises in the cavity field [cf. Eq. (5)], which can be interpreted as a closed-loop dissipative
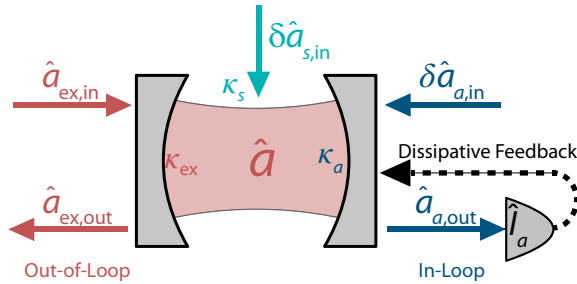

FIG. 1. Scheme for dissipative feedback in an optical microcavity. The intracavity field $\hat{a}$ is coupled to several different reservoirs, i.e., the laser input $\hat{a}_{\text{ex,in}}$, the vacuum noise from the scattering loss $\delta\hat{a}_{s,\text{in}}$ and the dissipative absorption $\delta\hat{a}_{a,\text{in}}$. The in-loop measurement of absorption field $\hat{a}_{a,\text{out}}$, results in the absorption flux $\hat{I}_a$, which is fed back to the optical cavity (black dashed curve). The out-of-loop measurement of $\hat{a}_{\text{ex,out}}$ is performed for coherent and incoherent spectroscopy.

feedback to the optical cavity field as shown in Fig. 1. The photon absorption can be described as an in-loop photodetection, which results in a feedback to the optical cavity, i.e., by changing the cavity frequency via the photothermal effect. The noise spectral density of the in-loop photon flux fluctuation δI_a, when normalized to shot noise, is given by

$$S_{\delta I_a}(\Omega) = |1 - \chi_{\text{fb}}(\Omega)|^{-2}, \quad (9)$$

where

$$\chi_{\text{fb}}(\Omega) = \sigma_d(\Omega)\kappa_a\left[\chi_{c,0}(\Omega) - \chi_{c,0}^*(-\Omega)\right]. \quad (10)$$

The dissipative feedback results in squashed or antisquashed in-loop optical field. We can obtain the *modified optical susceptibility*

$$\chi_{c,\text{eff}}(\Omega) = \chi_{c,0}(\Omega)/[1 - \chi_{\text{fb}}(\Omega)]. \quad (11)$$

In the case of $\bar{\Delta} \ll -\kappa$ i.e., when the pump is far red-detuned from the cavity resonance, the PSD of the in-loop photon flux at $\Omega \sim |\bar{\Delta}|$ is

$$S_{\delta I_a}(\Omega) \simeq \left|1 - \frac{2\bar{n}_c\kappa_a g_a g_{\text{th}}}{\Omega\kappa}\right|^{-2}, \quad (12)$$

and the effective optical susceptibility can be further simplified,

$$\chi_{c,\text{eff}}(\Omega) = \frac{1}{\kappa_{\text{eff}}/2 - i(\bar{\Delta}_{\text{eff}} + \Omega)}, \quad (13)$$

with a modified effective cavity linewidth

$$\kappa_{\text{eff}} = \kappa - 2\kappa_a \text{Re}[\sigma_d(\Omega)], \quad (14)$$

and a modified effective detuning

$$\bar{\Delta}_{\text{eff}} = \bar{\Delta} + \kappa_a \text{Im}[\sigma_d(\Omega)], \quad (15)$$

where $\bar{\Delta} = \Delta - \bar{n}_c g_a\kappa_a g_{\text{th}}/\gamma_{\text{th}}$. Due to the squashed or antisquashed absorbed photon fluctuations, *the dissipative feedback leads to modified cavity susceptibility for an input probing field*. In practice, the photothermal coefficient g_{th} can have different signs at room temperatures and cryogenic temperatures for different materials. For $g_{\text{th}} < 0$, we have $\kappa_{\text{eff}} > \kappa$ and $\bar{\Delta}_{\text{eff}} > \bar{\Delta}$; while for $g_{\text{th}} > 0$, we have $\kappa_{\text{eff}} < \kappa$ and $\bar{\Delta}_{\text{eff}} < \bar{\Delta}$.

As shown in Eq. (5), the intracavity field is coupled to an effective dissipative reservoir $\delta\hat{a}_d$. Different from the vacuum noise, the noise operator for the dissipative reservoir $\delta\hat{a}_d$ satisfies the following correlations:

$$\langle\delta\hat{a}_d^\dagger(\Omega)\delta\hat{a}_d(\Omega')\rangle = -\sigma_d(\Omega)\sigma_d(\Omega')\delta(\Omega + \Omega')2\pi$$
$$\langle\delta\hat{a}_d(\Omega)\delta\hat{a}_d^\dagger(\Omega')\rangle = [1 - \sigma_d(\Omega)][1 + \sigma_d(\Omega')]\delta(\Omega + \Omega')2\pi, \quad (16)$$

which may result in incoherent excess noise and noise correlations for the intracavity field.

To give an example, we show how the dissipative feedback can result in modified cavity susceptibility and excess noise correlations in the interferometric quantum optomechanical measurements. In such a cavity optomechanical system, a mechanical mode of frequency Ω_m is dispersively coupled to an optical mode of frequency ω_c at a vacuum optomechanical coupling rate of g_0 via radiation pressure. A cooling tone is applied close to the cavity red sideband, i.e., $\bar{\Delta} \simeq -\Omega_m$. The cooling tone gives rises to cavity enhanced anti-Stokes scattering of thermomechanical sideband around the cavity resonance. In the weak coupling regime, we can linearize the mechanical displacement $\hat{b} \to \bar{b} + \delta\hat{b}$. In the resolved-sideband regime, i.e., $\kappa \ll \Omega_m$, we can obtain the quantum Langevin equations for the field fluctuations in the rotating frame of the cooling tone. Within the rotating-wave approximation, we obtain,

$$\chi_{c,\text{eff}}^{-1}(\Omega)\delta\hat{a} = ig_0\bar{a}\delta\hat{b} + \sqrt{\kappa_a}\delta\hat{a}_d + \sqrt{\kappa_{\text{ex}}}\delta\hat{a}_{\text{ex,in}} + \sqrt{\kappa_s}\delta\hat{a}_{s,\text{in}}$$

$$\chi_m^{-1}(\Omega)\delta\hat{b} = ig_0\bar{a}\delta\hat{a} + \sqrt{\Gamma_m}\delta\hat{b}_{\text{in}} \qquad (17)$$

with mechanical susceptibility $\chi_m(\Omega) = 1/[\Gamma_m - i(\Omega - \Omega_m)]$ and $\chi_{c,\text{eff}}$ as defined in Eq. (13).

Both coherent and incoherent optomechanical spectroscopy of the out-of-loop optical field can be adopted for the measurement of the mechanical motion [31,32]. In a coherent spectroscopy, a weak probing tone is generated from the strong pumping tone, e.g., via an electro-optical-modulator, with frequency separation set by the microwave tone. The reflected light from the cavity is sent to the photodetector directly. The photocurrent is demodulated at the microwave frequency, from which we can obtain a coherent cavity response with the probing tone sweeping across the optical microcavity resonance. The cavity susceptibility is modified by the mechanical motion,

$$\chi_{c,\text{om}}(\Omega) = \frac{1}{\kappa_{\text{eff}}/2 - i(\bar{\Delta}_{\text{eff}} + \Omega) + \bar{n}_c g_0^2 \chi_m(\Omega)}. \qquad (18)$$

The mechanical motion leads to a destructive interference in the out-of-loop optical field. The coherent optomechanical spectroscopy of the cavity field results in the optomechanically-induced transparency [78,79]. The dynamical backaction results in a modified mechanical susceptibility, $\chi_{m,\text{eff}}(\Omega) = 1/[\Gamma_{\text{eff}}/2 - i(\Omega - \Omega_m)]$, with effective mechanical linewidth $\Gamma_{\text{eff}}(\Omega) = \Gamma_m + \Gamma_{\text{opt}}(\Omega)$ and optomechanical damping rate $\Gamma_{\text{opt}}(\Omega) = \kappa_{\text{eff}}\bar{n}_c g_0^2 |\chi_{c,\text{eff}}(\Omega)|^2$.

For $g_{\text{th}} > 0$, i.e., temperature increase results in blue shift of optical cavity frequency, the in-loop photon fluctuation is enhanced, i.e., $S_{\delta I_a}(\Omega_m) > 1$. This accordingly results in a decreased κ_{eff} and an increased optomechanical damping rate. For $\Omega_m \gg \gamma_{\text{th}}$, such as in an OMC, the effective detuning change due to the dissipative feedback is negligible, i.e., $\bar{\Delta}_{\text{eff}} \simeq \bar{\Delta}$. We note that, the photothermal effects can also change the mechanical susceptibility

by heating the mechanical oscillators [19,20,80], which is not considered here in our analysis. The coherent dissipative dynamics has been shown to introduce Floquet dynamics in quantum measurement of mechanical motion [31] and photothermal-induced transparency [81]. A similar mechanism has been reported in a membrane in the middle system with active feedback [73–75]. This can give rise to enhanced sideband cooling and even normal-mode splitting in a weakly coupled optomechanical system.

The coupling to the dissipative reservoir $\delta\hat{a}_d$ can introduce excess noise to the mechanical motion. In the resolved-sideband limit, the minimum final occupancy is obtained with $\bar{\Delta}_{\text{eff}} = -\Omega_m$, and takes the form,

$$\bar{n}_f = \frac{\bar{n}_{\text{th}}\Gamma_m + 4\bar{n}_l\bar{n}_c g_0^2/\kappa_{\text{eff}}}{\Gamma_m + 4\bar{n}_c g_0^2/\kappa_{\text{eff}}}, \qquad (19)$$

with

$$\bar{n}_l = \kappa_a \bar{n}_c^2 \sigma_0^2(\Omega_m)/\kappa_{\text{eff}}, \qquad (20)$$

being the limit of sideband cooling in the presence of the dissipative feedback. The dissipative feedback gives rise to an effective backaction heating of the mechanical motion. In the high cooperativity limit, i.e., $\Gamma_{\text{opt}} \gg \bar{n}_{\text{th}}\Gamma_m$, the final occupancy is limited by $\bar{n}_l$, due to the absorption-induced dissipative feedback.

In an incoherent optomechanical spectroscopy, the output field $\delta\hat{a}_{\text{ex,out}} = \delta\hat{a}_{\text{ex,in}} - \sqrt{\kappa_{\text{ex}}}\delta\hat{a}$, can be linearly measured by a quantum-limited balanced homodyne (heterodyne) detection by beating with a strong local oscillator. In the balanced heterodyne detection (BHD), the local oscillator of frequency ω_{LO} is placed on the blue side of the pump with a frequency separation close to the mechanical frequency. In an ideal detection, the symmetrized noise power spectral density (PSD) of the output photocurrent from BHD when normalized to the shot noise floor, takes the form,

$$S_I(\Omega + \Delta_{\text{LO}}) = \frac{\kappa_{\text{ex}}}{\kappa_{\text{eff}}}\Gamma_{\text{opt}}(\Omega + \Omega_m)\Gamma_{\text{eff}}|\chi_{m,\text{eff}}(\Omega + \Omega_m)|^2$$

$$\times (\bar{n}_f - 2\bar{n}_l) + 1 + 4\bar{n}_l\frac{\kappa_{\text{ex}}}{\kappa_{\text{eff}}}, \qquad (21)$$

assuming $\Delta_{\text{LO}} = \Omega_m + \omega_L - \omega_{\text{LO}} > 0$. Unanticipated *excess classical correlation* between measurement imprecision and backaction arises due to the dissipative dynamics, which can even lead to *noise squashing*, i.e., when $\bar{n}_f < 2\bar{n}_l$. In addition, the dissipative feedback results in an *increased noise floor,* i.e., $4\bar{n}_l\kappa_{\text{ex}}/\kappa_{\text{eff}}$, and *an effective detection efficiency* of $\kappa_{\text{ex}}/\kappa_{\text{eff}}$ as opposed to $\kappa_{\text{ex}}/\kappa$.

We note that, both Eqs. (19) and (21) exhibit some similarities to an optomechanical system sideband cooled by a laser with excess noise, which also introduces excess backaction heating and classical correlations [26–28,47,48]. The incoherent dissipative dynamics

is mediated via absorption-induced cavity frequency fluctuation, by replacing the vacuum noise with excess backaction heating $\Gamma_{\text{opt}}\bar{n}_l / \Gamma_{\text{eff}}$ approximately quadratic in $\bar{n}_c$ [cf. Eq. (19)]. Surprisingly, even in the absence of excess laser noise, the phonon occupancy can be *underestimated* due to the excess classical correlation from the dissipative reservoir in the mechanical noise thermometry.

II. EXPERIMENTAL RESULTS

We observe the dissipative dynamics on cavity linewidth, cooling rate, and noise floor caused by photon absorption in an optomechanical spectroscopy of sideband-cooled OMCs with different optical losses at cryogenic temperature in vacuum and under ambient conditions, respectively. In a typical OMC, an optical mode at wavelength of approximately 1550 nm is coupled to a colocalized mechanical mode of $\Omega_m/2\pi$ approximately 5

GHz at a vacuum optomechanical coupling rate of $g_0/2\pi$ approximately 1 MHz. Laser light is evanescently coupled into the OMC from a tapered optical fiber via a coupling waveguide, with a waveguide coupling efficiency η_{wg} ranging from 40% to 60%. The reflected light from the OMC is collected for optomechanical spectroscopy. More details of the OMCs and the experimental setup are in Appendix B.

In the first set of measurements, we place an OMC device of $\kappa/2\pi$ approximately 1.7 GHz (used in Refs. [31, 33]) in a ^{3}He buffer gas cryostat (Oxford Instruments HelioxTL). The experiments are performed at approximately 8 K under vacuum (pressure approximately 0.5 mbar), in contrast to previous experiments benefiting from the better thermalization due to gaseous ^{3}He [31,33]. In the coherent spectroscopy, the effective laser detuning $\bar{\Delta}_{\text{eff}}$ is manually adjusted to approximately $-\Omega_m$, to achieve optimal sideband cooling. In Fig. 2(a), the inferred κ_{eff}
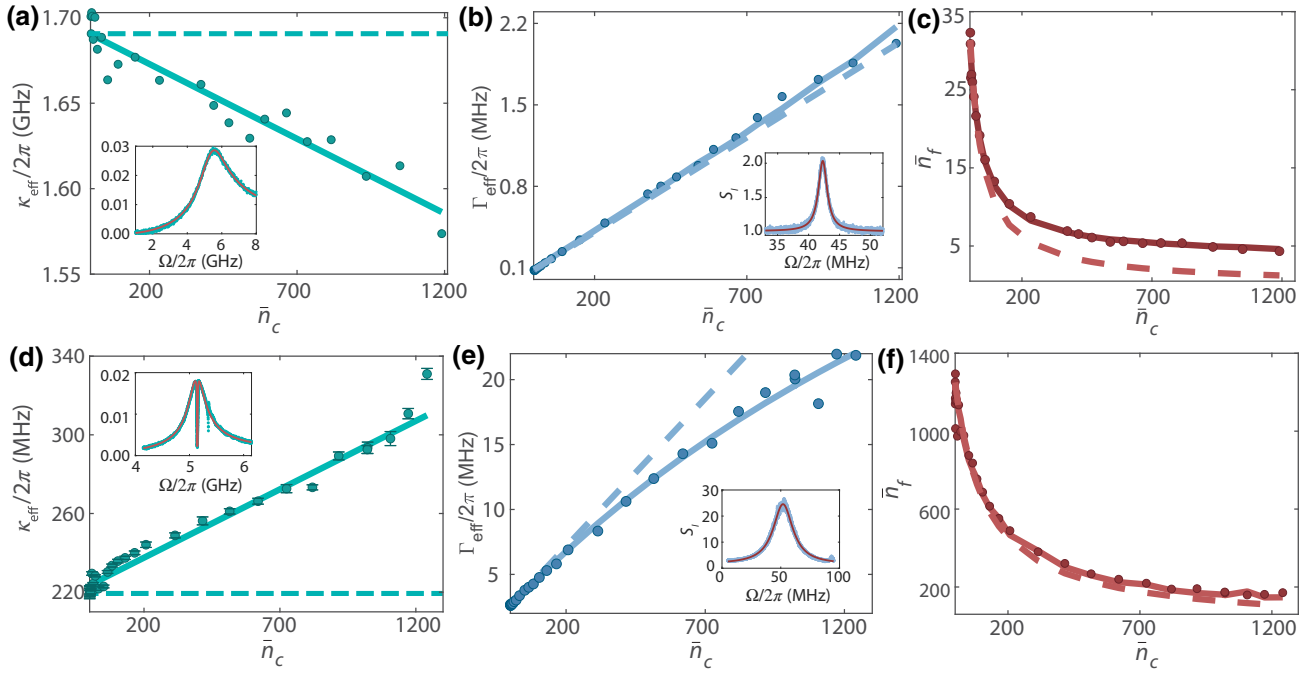

FIG. 2. Observation of dissipative feedback dynamics on cavity linewidth and optomechanical damping in optomechanical spectroscopy of two sideband-cooled OMCs under different conditions. In (a)–(c), we show the results for an OMC of $\kappa/2\pi \sim 1.7$ GHz at approximately 8 K with a pressure approximately 0.5 mbar. (a) Fitted effective optical linewidth κ_{eff} (green circles) versus intracavity photon number $\bar{n}_c$ in the coherent cavity spectroscopy. The green curve shows a fitting curve incorporating the coherent dissipative dynamics, revealing a cavity linewidth that reduces with $\bar{n}_c$. The green dashed line shows the original cavity linewidth. The inset shows a typical fitting of coherent cavity response. (b) Fitted effective mechanical linewidth Γ_{eff} (blue circles) in the incoherent balanced heterodyne noise spectrum versus $\bar{n}_c$. Blue curve shows a fitting curve incorporating κ_{eff} due to coherent dissipative dynamics. Blue dashed curve shows a theoretical plot without the dissipative absorption. The inset shows a typical fitting of incoherent noise spectrum. (c) Mean phonon occupancy $\bar{n}_f$ (red circles) from the incoherent noise spectrum via mechanical noise thermometry versus $\bar{n}_c$. The calibration is done using mechanical noise thermometry anchored at the lowest photon number. The red curve shows a fitting curve incorporating the effective optical linewidth change and linear absorption heating. The red dashed curve shows a theoretical plot without dissipative absorption. In (d)–(f), we show the results from an OMC of $\kappa/2\pi$ approximately 220 MHz at room temperature and pressure, corresponding to the data in (a)–(c). Here an increase of κ_{eff} versus $\bar{n}_c$ is observed due to the dissipative feedback. In (e), the green dashed line shows the ideal theoretical effective mechanical linewidth without dissipative dynamics. In (d), the error bars are from the fitting of the coherent cavity response, while in (a)–(c) and (e),(f) error bars are within the circles and thus are not shown.

from the coherent spectroscopy versus $\bar{n}_c$ are shown in green circles. Typically, the nonlinear dynamics in the cavity, such as two-photon absorption (TPA) and free-carrier absorption (FCA), may increase the cavity linewidth due to the cavity enhancement [82]. Counterintuitively, the inferred κ_{eff} decreases as the cooling tone $\bar{n}_c$ increases, as shown in Fig. 2(a). We attribute this to the dissipative dynamics, where the optical mode is coupled to an effective dissipative reservoir, with $g_{\mathrm{th}} > 0$ (blue shift of cavity frequency due to temperature increase) for silicon OMC at 8 K. The optical absorption and decreased thermal conductivity of silicon at low temperature result in the optical heating of the OMC. In Fig. 2(a), the green curve shows a linear fit using Eq. (14), which results in a fitted $\kappa_a \sigma_0(\Omega_m) \simeq 2\pi \times 44$ kHz. At the highest power ($\bar{n}_c = 1190$), *the inferred κ_{eff} is decreased by* approximately 7.5% *compared to the cavity linewidth κ*. In Fig. 2(b), the fitted Γ_{eff} from the incoherent noise spectrum in the BHD are shown in blue circles, with a light blue fitting curve incorporating κ_{eff}, which results in $g_0/2\pi = 829$ kHz and $\Gamma_m/2\pi = 81$ kHz. The effective damping rate is shown to be higher than the theoretical model without the absorption (the dashed blue curve), due to the increased optical susceptibility. In Fig. 2(c), we show the calibrated final phonon occupancy $\bar{n}_f$ from the BHD using standard mechanical noise thermometry by anchoring the noise spectrum at the lowest power, i.e., $\bar{n}_c = 1.4$. A fitting curve with a theoretical model incorporating linear absorption heating is shown in the light red curve [31]. The minimum phonon occupancy achieved is $\bar{n}_f \sim 4.3 \pm 0.1$ at $\bar{n}_c \sim 1200$.

In the second set of measurements, we perform an optomechanical spectroscopy of a sideband-cooled OMC of $\kappa/2\pi = 220$ MHz (used in Refs. [32,34]) at room temperature and pressure. In Fig. 2(d), the fitted κ_{eff} versus $\bar{n}_c$ are shown in green circles from the coherent cavity response measurement, with $\bar{\Delta}_{\mathrm{eff}} \simeq -\Omega_m$. At the highest powers, e.g., $\bar{n}_c \simeq 1110$, *the inferred κ_{eff} is increased by* approximately *half of the original κ*. Despite the low cavity loss, the dissipative dynamics arises due to the large thermorefractive coefficient and the cavity field enhancement. In Fig. 2(d), the light green curve shows a linear fitting using Eq. (14), which results in a fitted $\kappa_a \sigma_0(\Omega_m) \simeq -2\pi \times 35$ kHz. In Appendix D, we discuss additional possible nonlinear dynamics from TPA and FCA. In Fig. 1(e), we show the inferred Γ_{eff} from the BHD (blue circles), which deviates from the linear scaling of $\bar{n}_c$ (blue dashed curve). The light blue fitting curve incorporating κ_{eff} results in $g_0/2\pi = 1.12$ MHz and $\Gamma_m/2\pi = 2.56$ MHz. In Fig. 1(f), we show the calibrated $\bar{n}_f$ via mechanical noise thermometry, with the optomechanical damping rate incorporating κ_{eff}. The increased κ_{eff} at high powers results in an increased $\bar{n}_f$, with minimum $\bar{n}_f \sim 159 \pm 4$ at $\bar{n}_c = 1107$.

Figure 3 shows the noise floor in the incoherent noise spectrum from the two sets of measurements, normalized
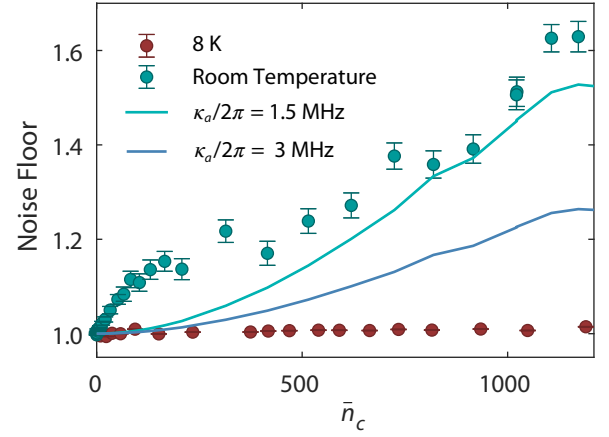

FIG. 3. Noise floor from the incoherent optomechanical spectroscopy of sideband-cooled OMCs at different intracavity photon numbers. The noise floor is normalized to the shot noise floor. The red circles correspond to the OMC with $\kappa/2\pi \sim 1.7$ GHz at approximately 8 K, while the green circles correspond to the OMC with $\kappa/2\pi \sim 220$ MHz under ambient conditions. The green and blue curves correspond to the theoretical plots for κ_a of $2\pi \times 1.5$ MHz and $2\pi \times 3$ MHz, incorporating the inferred κ_{eff} and $\kappa_a \sigma_0(\Omega_m)$ from coherent cavity response.

to the shot noise floor. The red circles correspond to the 8-K measurements, where the noise floor changes negligibly with $\bar{n}_c$. The green circles correspond to the room-temperature measurements, where the noise floor increases versus the optical power. The large error bars are due to the large SNR of the thermomechanical sideband at room temperature. We attribute the large noise floor increase to the dissipative dynamics, instead of the excess noise in the optical or electronic components in the setup, as detailed in Appendix D. Incorporating the fitted κ_{eff} and $\kappa_a \sigma_0(\Omega_m)$ from coherent response measurements at room temperature, we plot the theoretical curves of the noise floor assuming an absorption rate κ_a of $2\pi \times 3$ MHz (blue curve) and $2\pi \times 1.5$ MHz (green curve) in Fig. 3. In principle, κ_a can be obtained from κ_{eff} and the noise floor from the coherent and incoherent spectroscopy, and the excess classical correlation in the mechanical noise thermometry can be estimated accordingly. We observe large deviations of the increased noise floor at low powers, most likely due to the cavity frequency noise due to free-carrier absorption [82,83] as discussed in Appendix D. Due to the complicated cavity dynamics, the excess noise correlations are not quantified in our measurements.

III. OPTICAL KERR SQUEEZING

The dissipative feedback arises in optomechanical spectroscopy due to photon absorption. Such photothermal effects manifest as a Kerr-type nonlinearity [31], where the cavity frequency shift is proportional to the intracavity photon number. A Kerr medium has been suggested

as a QND device in a feedback loop to generate optical squeezing [22,76]. In such QND feedback, the intensity of in-loop optical field constitutes a measurement without quantum backaction, although phase fluctuations are added. The dissipative feedback is fundamentally different from a QND feedback, e.g., Kerr squeezing [22,76], as excess noise always arises in the out-of-loop field due to uncorrelated noise from the in-loop field detection, i.e., photon absorption.

Here we consider a microcavity with coexisting dissipative feedback via photothermal effects and Kerr nonlinearity (a situation encountered e.g. in Si_3N_4 microresonators). We can obtain the quantum Langevin equations of the field fluctuation in the frequency domain,

$$\chi_{c,0}^{-1}(\Omega)\delta\hat{a} = [\bar{n}_c\sigma_0(\Omega)\kappa_a - i\bar{n}_c g_{Kerr}](\delta\hat{a} + \delta\hat{a}^{\dagger})$$
$$+ \sqrt{\kappa_a}\delta\hat{a}_d + \sqrt{\kappa_{ex}}\delta\hat{a}_{ex,in} + \sqrt{\kappa_s}\delta\hat{a}_{s,in} \quad (22)$$

where g_{Kerr} is the single-photon nonlinear Kerr coupling rate [84] and $\chi_{c,0}(\Omega)$ is given by Eq. (6) with $\bar{\Delta} = \Delta - (g_a\kappa_a g_{th}/\gamma_{th} + g_{Kerr})\bar{n}_c$. We can obtain the symmetrized PSD of the out-of-loop field quadrature, $\hat{X}_\theta = \delta\hat{a}_{ex,out}e^{-i\theta} + \delta\hat{a}_{ex,out}^{\dagger}e^{i\theta}$, in a balanced homodyne detection, with LO of the pumping tone frequency and θ being the phase difference between the LO and the pump. We focus on the simple case where the laser detuning $\bar{\Delta} = 0$. For Kerr squeezing, i.e., $g_{th} = 0$, the PSD takes the form,

$$S_{I,Kerr}(\Omega) = 1 - \frac{16\bar{n}_c\eta_c\kappa\sin(\theta)g_{Kerr}\left[(\kappa^2 + 4\Omega^2)\cos(\theta) - 4\bar{n}_c\kappa\sin(\theta)g_{Kerr}\right]}{(\kappa^2 + 4\Omega^2)^2}. \quad (23)$$

where we assume an ideal detection and $\eta_c = \kappa_{ex}/\kappa$. Such QND feedback can result in Kerr squeezing in the output field for an optical quadrature with minimum variance below the vacuum noise at an optimal angle, as detailed in Appendix A. In contrast, for dissipative dynamics only, i.e., $g_{Kerr} = 0$, the PSD takes the form, $S_{I,a}(\Omega) = 1 + S_{I,a}^{ex}(\Omega)$, where the incoherent optical absorption always results in an excess noise, i.e., the photothermal noise,

$$S_{I,a}^{ex}(\Omega) = \frac{16\bar{n}_c\kappa_a\kappa_{ex}\sin(\theta)^2 g_a^2 g_{th}^2}{(\kappa^2 + 4\Omega^2)(\Omega^2 + \gamma_{th}^2)} \geq 0. \quad (24)$$

We note that, this coincides with earlier experimental and theoretical works in optical systems with intensity feedback, where in-loop photocurrent can be squashed while the out-of-loop photocurrent always becomes antisquashed [23–25]. The Kerr nonlinearity on the other hand, constitutes a QND detection of the in-loop optical field, which enables Kerr squeezing in the out-of-loop field, which enables the Kerr squeezing in the out-of-loop field, as expected [22,76].

When Kerr nonlinearity and dissipative dynamics coexist, the total PSD is given by $S_I(\Omega) = S_{I,Kerr}(\Omega) + S_{I,tot}^{ex}(\Omega)$, with total excess noise $S_{I,tot}^{ex}(\Omega) = S_{I,a}^{ex}(\Omega) + S_{I,c}^{ex}(\Omega)$ due to the dissipative dynamics. The coherent dissipative dynamics gives arises to,

$$S_{I,c}^{ex}(\Omega) = \frac{64\bar{n}_c^2\kappa_a\kappa_{ex}g_a g_{Kerr}g_{th}\sin^2(\theta)\left(\kappa\gamma_{th} - 2\Omega^2\right)}{\left(\kappa^2 + 4\Omega^2\right)^2\left(\gamma_{th}^2 + \Omega^2\right)}, \quad (25)$$

We note that, when $g_a g_{th}\left(\kappa^2 + 4\Omega^2\right) < g_{Kerr}\left(8\Omega^2 - 4\kappa\gamma_{th}\right)$, the total excess noise $S_{I,tot}^{ex} < 0$, which *opens an interesting regime for dissipation improved Kerr squeezing.*

In Fig. 4, we show the theoretical curves of estimated Kerr squeezing in a state-of-the-art Si_3N_4 microring resonators at optimal squeezing angles with realistic
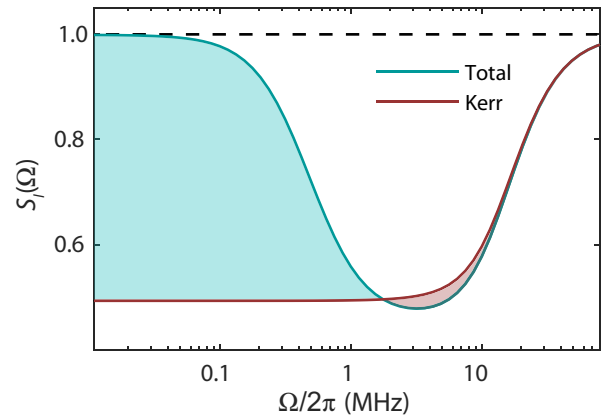

FIG. 4. Estimated Kerr squeezing with dissipative dynamics at optimal angles in a Si_3N_4 microcavity. The noise spectral density is normalized to the shot noise floor (black dashed line). The red curve corresponds to the case where the dissipative dynamics is absent, while the green curve corresponds to the case where Kerr nonlinearity and dissipative dynamics coexist. The green and red shade areas correspond to the excess noise and improved squeezing due to dissipative feedback. (Parameters: $\kappa/2\pi = 15$ MHz, $\kappa_{ex}/2\pi = 8$ MHz, $\kappa_a/2\pi = 6$ MHz, $\kappa_s/2\pi = 1$ MHz, $\gamma_{th}/2\pi = 20$ kHz, $g_a g_{th}/2\pi = -0.05$ Hz, $g_{Kerr}/2\pi = -0.5$ Hz, and $\bar{n}_c = 10^7$).

parameters [8]. The Kerr nonlinearity in such a microring resonator can lead to frequency comb and dissipative soliton generation at low pumping powers (approximately mW) [2], due to the extremely low optical loss ($\kappa/2\pi <$ 20 MHz). The red curve includes only Kerr nonlinearity while the green curve considers both the Kerr nonlinearity and the dissipative dynamics. As shown in Fig. 4, the green curve exhibits excess noise at low frequencies due to the incoherent dissipative dynamics, while showing a slight improvement of Kerr squeezing at frequencies between 2–10 MHz due to the coherent dissipative dynamics. In practice, the Kerr squeezing is limited by the detection efficiency and the thermorefractive noise [85–87].

IV. CONCLUSION

We observe the dissipative dynamics resulting from photon absorption in quantum optomechanical spectroscopy of sideband-cooled optomechanical crystal cavities under different conditions and develop a theoretical model for our experimental observations. Such dissipative dynamics comes from a dissipative quantum feedback to the optical cavity. The in-loop detection of the optical absorption field results in a modified optical susceptibility, and results in excess noise correlations in the quantum measurement of mechanical motion. Such dissipative feedback differs from the quantum nondemolition feedback, e.g., Kerr squeezing. The observed dynamics is applicable to any dissipative feedback in the cavities of different bandwidths, such as TPA, FCA, and photorefractive effects [88]. It offers crucial understanding to cavity spectroscopy in both optical and superconducting microwave microcavities, such as noise thermometry, quantum enhanced sensing, and microwave-optical frequency conversions [89,90]. While our study has experimentally considered the optical domain, it is worth pointing out, that our results also apply to the microwave domain, as studied in circuit optomechanics or used in superconducting circuits based research [4,91]. While it is well known that TLS can lead to a drive power dependent quality factor of superconducting microwave cavities, the described phenomena may be applicable to mechanisms, which result in power or temperature-dependent cavity frequencies, e.g., due to quasiparticles [92–95]. The dissipative feedback can also be exploited for future dissipation engineering, such as enhanced sideband cooling and Kerr squeezing, and nonreciprocal photonic devices.

All data and analysis files are available online [96].

APPENDIX A: THEORY

1. Optomechanical spectroscopy

For laser sideband cooling in a resolved-sideband optomechanical system coupled to a dissipative reservoir, the quantum Langevin equation takes the form,

$$\chi_{c,\text{eff}}^{-1}(\Omega)\delta\hat{a} = ig_0\bar{a}\delta\hat{b} + \sqrt{\kappa_a}\delta\hat{a}_d + \sqrt{\kappa_{\text{ex}}}\delta\hat{a}_{\text{ex,in}} + \sqrt{\kappa_s}\delta\hat{a}_{s,\text{in}}$$

$$\chi_m^{-1}(\Omega)\delta\hat{b} = ig_0\bar{a}\delta\hat{a} + \sqrt{\Gamma_m}\delta\hat{b}_{\text{in}} \tag{A1}$$

and the noise operators satisfy the following correlations:

$$\left\langle \delta\hat{a}_{\text{ex,in}}^\dagger(\Omega)\delta\hat{a}_{\text{ex,in}}(\Omega')\right\rangle = 0,$$
$$\left\langle \delta\hat{a}_{\text{ex,in}}(\Omega)\delta\hat{a}_{\text{ex,in}}^\dagger(\Omega')\right\rangle = \delta(\Omega+\Omega')2\pi,$$
$$\left\langle \delta\hat{a}_{0,\text{in}}^\dagger(\Omega)\delta\hat{a}_{0,\text{in}}(\Omega')\right\rangle = 0,$$
$$\left\langle \delta\hat{a}_{0,\text{in}}(\Omega)\delta\hat{a}_{0,\text{in}}^\dagger(\Omega')\right\rangle = \delta(\Omega+\Omega')2\pi,$$
$$\left\langle \delta\hat{b}_{\text{in}}^\dagger(\Omega)\delta\hat{b}_{\text{in}}(\Omega')\right\rangle = \bar{n}_{\text{th}}\delta(\Omega+\Omega')2\pi,$$
$$\left\langle \delta\hat{b}_{\text{in}}(\Omega)\delta\hat{b}_{\text{in}}^\dagger(\Omega')\right\rangle = (\bar{n}_{\text{th}}+1)\delta(\Omega+\Omega')2\pi. \tag{A2}$$

In addition, the noise operator for the dissipative reservoir satisfies the following correlations:

$$\left\langle \delta\hat{a}_d^\dagger(\Omega)\delta\hat{a}_d(\Omega')\right\rangle = -\sigma_d(\Omega)\sigma_d(\Omega')\delta(\Omega+\Omega')2\pi,$$
$$\left\langle \delta\hat{a}_d(\Omega)\delta\hat{a}_d^\dagger(\Omega')\right\rangle = [1-\sigma_d(\Omega)][1+\sigma_d(\Omega')]\delta(\Omega+\Omega')2\pi,$$
$$\left\langle \delta\hat{a}_d(\Omega)\delta\hat{a}_d(\Omega')\right\rangle = -[1-\sigma_d(\Omega)]\sigma_d(\Omega')\delta(\Omega+\Omega')2\pi,$$
$$\left\langle \delta\hat{a}_d^\dagger(\Omega)\delta\hat{a}_d^\dagger(\Omega')\right\rangle = \sigma_d(\Omega)[1+\sigma_d(\Omega')]\delta(\Omega+\Omega')2\pi. \tag{A3}$$

We can obtain the noise spectrum of the mechanical oscillator,

$$S_{\hat{b}\hat{b}}(\Omega) = \int_{-\infty}^\infty \left\langle \delta\hat{b}^\dagger(t)\delta\hat{b}(t')\right\rangle e^{i\Omega t}dt$$
$$= (\bar{n}_{\text{th}}\Gamma_m + \Gamma_+)|\chi_{\text{eff}}(-\Omega)|^2 \tag{A4}$$

where $\Gamma_+ = \bar{n}_c g_0^2 |\chi_c(\Omega_m)|^2 \kappa_a \sigma_d^2$, and

$$S_{\hat{b}^\dagger\hat{b}^\dagger}(\Omega) = \int_{-\infty}^\infty \left\langle \delta\hat{b}(t)\delta\hat{b}^\dagger(t')\right\rangle e^{i\Omega t}dt$$
$$= [(\bar{n}_{\text{th}}+1)\Gamma_m + \Gamma_-]|\chi_{\text{eff}}(\Omega)|^2 \tag{A5}$$

where $\Gamma_- = \bar{n}_c g_0^2 |\chi_c(\Omega_m)|^2 (\kappa_{\text{eff}} + \kappa_a \sigma_d^2)$. The two-sided mechanical noise spectrum can be obtained,

$$S_{\hat{x}\hat{x}}(\Omega)/x_{\text{zpf}}^2 = S_{\hat{b}^\dagger \hat{b}^\dagger}(\Omega) + S_{\hat{b}\hat{b}}(\Omega)$$
$$= \Gamma_{\text{eff}}\left[|\chi_{\text{eff}}(\Omega)|^2(\bar{n}_f + 1) + |\chi_{\text{eff}}(-\Omega)|^2 \bar{n}_f\right], \tag{A6}$$

where the final occupancy takes the form,

$$\bar{n}_f = \frac{\bar{n}_{\text{th}}\Gamma_m + \Gamma_{\text{opt}}\bar{n}_l}{\Gamma_{\text{eff}}}, \tag{A7}$$

with $\Gamma_{\text{opt}} = \kappa_{\text{eff}}\bar{n}_c g_0^2 |\chi_{c,\text{eff}}(\Omega)|^2$ and $\bar{n}_l = \kappa_a \bar{n}_c^2 \sigma_0^2/\kappa_{\text{eff}}$. The coupling to the dissipative reservoir results in excess backaction heating of the mechanical oscillator. In a balanced heterodyne measurement, the output field is beating with a strong LO of frequency ω_{LO}, which is placed on the blue side of the pumping tone with a frequency separation close to the mechanical frequency. The symmetrized PSD of the photocurrent from the BHD is given by, $S_I(\Omega) = \frac{1}{2}\int_{-\infty}^{\infty}\langle\{\delta I(t+t'),\delta I(t')\}\rangle e^{i\Omega t}dt$. In practice, there are other losses in the photodetection, such as in the fiber or the photodetection, resulting in a limited external detection efficiency η_{ex}. Under optimal sideband cooling condition, i.e., $\bar{\Delta}_{\text{eff}} = -\Omega_m$, the photocurrent PSD, when normalized to the shot noise floor, is given by,

$$S_I(\Omega + \Delta_{\text{LO}}) = \eta_{\text{ex}}\frac{4\kappa_{\text{ex}}\bar{n}_c g_0^2}{\kappa_{\text{eff}}^2}\Gamma_{\text{eff}}|\chi_{m,\text{eff}}(\Omega + \Omega_m)|^2$$
$$\times (\bar{n}_f - 2\bar{n}_l) + 1 + 4\eta_{\text{ex}}\bar{n}_l\frac{\kappa_{\text{ex}}}{\kappa_{\text{eff}}}, \tag{A8}$$

with $\Delta_{\text{LO}} = \Omega_m + \omega_L - \omega_{\text{LO}} > 0$ and $\Gamma_{\text{eff}} = \Gamma_m + 4\bar{n}_c g_0^2/\kappa_{\text{eff}}$. At low cooling power, the signal-to-noise ratio of the thermomechanical sideband is given by,

$$\text{SNR} = \frac{16\eta_{\text{ex}}\bar{n}_c g_0^2 \kappa_{\text{ex}} k_B T}{\kappa^2 \Gamma_m \hbar \Omega_m}, \tag{A9}$$

with bath temperature T and negligible dynamical backaction. In the fitting of $\bar{n}_c$-dependent Γ_{eff} in the main text, the inferred κ_{eff} is incorporated, with g_0 and Γ_m as free fitting parameters. The mechanical noise thermometry can be performed by anchoring the phonon occupancy to the lowest power via Eq. (A8), incorporating the inferred κ_{eff} in

the optomechanical damping rate. The external detection efficiency η_{ex} can be obtained accordingly, and is estimated to be approximately 0.15 in the room-temperature experiments. The dissipative dynamics results in an excess noise above the shot noise floor

$$S_{I,\text{ex}}(\Omega + \Delta_{\text{LO}}) = 4\eta_{\text{ex}}\bar{n}_l\frac{\kappa_{\text{ex}}}{\kappa_{\text{eff}}} = \frac{4\eta_{\text{ex}}\kappa_a\kappa_{\text{ex}}\bar{n}_c^2\sigma_0^2}{\kappa_{\text{eff}}^2}. \tag{A10}$$

However, Eq. (A10) is not sufficient to fully capture the observed noise increase, which may be partially from the cavity frequency noise due to free-carrier absorption [82, 83]. For the fitting of $\bar{n}_c$-dependent $\bar{n}_f$ in the main text, we incorporate a linear optical absorption for the mechanical motion, as in Ref. [31].

2. Optical Kerr squeezing

The Kerr nonlinearity coupling rate in the main text can be estimated through [84]

$$g_{\text{Kerr}} = -\omega_c\frac{n_2}{n_0}\frac{\hbar\omega_c c}{V_{\text{mode}}n_0} < 0, \tag{A11}$$

where n_0 is the linear refractive index, n_2 the Kerr coefficient, V_{mode} the effective mode volume of the cavity, and c the speed of light. The output field quadrature can be linearly measured in a balanced homodyne detection, by beating with a strong LO of the pumping tone frequency. This results in the photocurrent fluctuation, $\delta\hat{I}(t) = |\bar{a}_{\text{LO}}|\hat{X}_\theta$, where θ is the phase difference between the LO and pumping tone. The symmetrized noise PSD of the output photocurrent, when normalized to the shot-noise floor, is

$$S_I(\Omega) = \left\langle\hat{X}_\theta(-\Omega)\hat{X}_\theta(\Omega)\right\rangle_s$$
$$= \frac{1}{2}\left(\left\langle\hat{X}_\theta(-\Omega)\hat{X}_\theta(\Omega)\right\rangle + \left\langle\hat{X}_\theta(\Omega)\hat{X}_\theta(-\Omega)\right\rangle\right). \tag{A12}$$

The full expression of the PSD can be obtained analytically, which is too complicated to be presented here. We focus on the simple case where the laser detuning $\bar{\Delta} = 0$. In the absence of the dissipative dynamics, i.e., $g_{\text{th}} = 0$, the PSD takes the form,

$$S_{I,\text{Kerr}}(\Omega) = 1 - \frac{16\bar{n}_c\eta_{\text{ex}}\eta_c\kappa\sin(\theta)g_{\text{Kerr}}\left[(\kappa^2 + 4\Omega^2)\cos(\theta) - 4\bar{n}_c\kappa\sin(\theta)g_{\text{Kerr}}\right]}{(\kappa^2 + 4\Omega^2)^2}. \tag{A13}$$

with cavity coupling efficiency $\eta_c = \kappa_{ex}/\kappa$ and external detection efficiency η_{ex}. The minimum PSD,

$$S_{I,\text{Kerr}}^{\min}(\Omega) = 1 - \frac{2\eta_{ex}\eta_c}{\sqrt{\left[(\kappa^2 + 4\Omega^2)/4\bar{n}_c\kappa g_{\text{Kerr}}\right]^2 + 1} + 1},$$
(A14)

which is limited by the cavity linewidth and total detection efficiency $\eta_{ex}\eta_c$, can be obtained at $\theta_{\text{opt}}(\Omega) = \tan^{-1}\left[(\kappa^2 + 4\Omega^2)/4\bar{n}_c\kappa g_{\text{Kerr}}\right]/2$. In the absence of the Kerr nonlinearity, i.e., $g_{\text{Kerr}} = 0$, the PSD takes the form $S_{I,a}(\Omega) = 1 + S_{I,a}^{ex}(\Omega)$, where the incoherent dissipative dynamics always results in an excess noise,

$$S_{I,a}^{ex}(\Omega) = \frac{16\bar{n}_c\eta_{ex}\eta_a\eta_c\kappa^2\sin(\theta)^2 g_a^2 g_{\text{th}}^2}{(\kappa^2 + 4\Omega^2)(\Omega^2 + \gamma_{\text{th}}^2)} \geq 0, \quad (A15)$$

with $\eta_a = \kappa_a/\kappa$.

In most optical systems, the Kerr nonlinearity and dissipative dynamics coexist, the total PSD is given by

$$S_I(\Omega) = S_{I,\text{Kerr}}(\Omega) + S_{I,\text{tot}}^{ex}(\Omega), \quad (A16)$$

with total excess noise $S_{I,\text{tot}}^{ex}(\Omega) = S_{I,a}^{ex}(\Omega) + S_{I,c}^{ex}(\Omega)$ due to the absorption. The *coherent dissipative dynamics* gives rise to,

$$S_{I,c}^{ex}(\Omega) = \frac{64\bar{n}_c^2\eta_{ex}\eta_a\eta_c\kappa^2 g_a g_{\text{Kerr}} g_{\text{th}}\sin^2(\theta)\left(\kappa\gamma_{\text{th}} - 2\Omega^2\right)}{\left(\kappa^2 + 4\Omega^2\right)^2\left(\gamma_{\text{th}}^2 + \Omega^2\right)}.$$
(A17)

The minimum quadrature can be obtained accordingly at the frequency-dependent optimal squeezing angle,

$$\theta_{\text{opt}}(\Omega) = \begin{cases} \dfrac{\arctan(-B/A)}{2} & A < 0 \\ \dfrac{\arctan(-B/A) + \pi}{2} & A > 0 \end{cases}, \quad (A18)$$

where

$$A = \bar{n}_c\kappa\left[4\eta_a g_a g_{\text{Kerr}} g_{\text{th}}\left(2\Omega^2 - \kappa\gamma_{\text{th}}\right) - \eta_a g_a^2 g_{\text{th}}^2\left(\kappa^2 + 4\Omega^2\right)\right.$$
$$\left. - 4g_{\text{Kerr}}^2\left(\gamma_{\text{th}}^2 + \Omega^2\right)\right]/g_{\text{Kerr}},$$
$$B = \left(\kappa^2 + 4\Omega^2\right)\left(\gamma_{\text{th}}^2 + \Omega^2\right) > 0. \quad (A19)$$

We note that, when $g_a g_{\text{th}}\left(\kappa^2 + 4\Omega^2\right) < g_{\text{Kerr}}\left(8\Omega^2 - 4\kappa\gamma_{\text{th}}\right)$, the total excess noise $S_{I,\text{tot}}^{ex} < 0$. This brings about an interesting regime for dissipation-assisted Kerr squeezing.

APPENDIX B: SAMPLE AND EXPERIMENTAL DETAILS

Both OMCs in the main text are fabricated on a silicon-on-insulator wafer (Soitec) with a top-silicon device-layer thickness of 220 nm and a buried-oxide layer thickness of 2 μm. The OMC with $\kappa/2\pi = 1.6$ GHz, is patterned by electron-beam lithography (EBL) using ZEP520A (100%) as a positive resist. The pattern is transferred to the device layer following a reactive ion etching using SF6/C4F8 plasma [31,33]. The OMC of $\kappa/2\pi = 220$ MHz, is patterned by using EBL using 4% hydrogen silsesquioxane (HSQ) as a negative resist. Pattern transfer into the device layer is accomplished by inductively-coupled-plasma reactive ion etching (ICP RIE) using HBr/O$_2$ [32,34]. To permit input-output coupling with a tapered fiber, an additional photolithography step is performed for both OMCs followed by RIE with a mixture of SF$_6$ and C$_4$F$_8$ to create a mesa structure. After resist removal, the buried oxide layer is partially removed in 10% hydrofluoric acid to create free-standing devices. A Piranha (a mixture of sulfuric acid and hydrogen peroxide) cleaning step is performed to remove organic residues. In the end, the sample is dipped into 2% hydrofluoric acid to terminate the silicon surface with hydrogen atoms.

The characterized parameters for the two OMCs under different measurement conditions are listed in Table I. The measurement of the OMC of $\kappa/2\pi = 1.6$ GHz is performed in a ^{3}He buffer gas cryostat (Oxford Instruments HelioxTL). As shown in our previous experiments, the gaseous ^{3}He improves the thermalization of the silicon OMC significantly. In this experiment, the pressure of buffer gas is reduced to approximately 0.5 mbar with the cryostat temperature stabilized around 8 K, resulting in significant optical absorption heating.

In Fig. 5, we show the experimental setup for the optomechanical spectroscopy. Laser light from the ECDL passes through a phase modulator. A pair of weak probing tones is generated, with frequency separation set by a microwave tone from a vector network analyzer (VNA). Light is coupled into the OMC with a tapered optical fiber. The reflected light from the OMC is collected for optomechanical spectroscopy. In the coherent spectroscopy, the photocurrent of the reflected light is sent to the VNA and demodulated at the microwave frequency, resulting

TABLE I. Detailed characterized parameters of the two tested OMC devices D1 and D2. D1 is measured at approximately 8 K with a pressure of 0.5 mbar, while D2 is measured at ambient conditions.

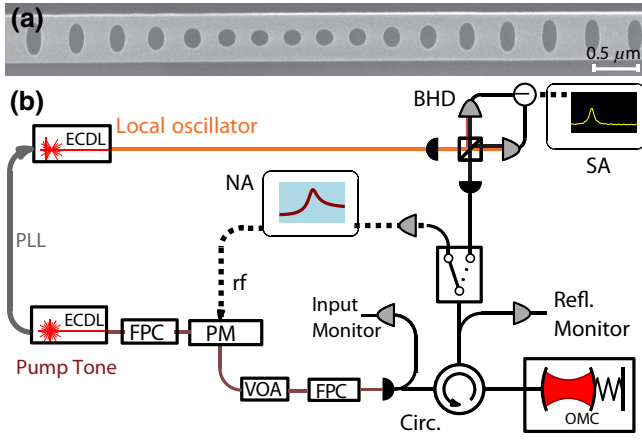|	λ (nm)	$\kappa/2\pi$	$\kappa_{ex}/2\pi$	η_{wg}	$\Omega_m/2\pi$	$\Gamma_m/2\pi$	$g_0/2\pi$
D1	1540	1.7 GHz	0.5 GHz	0.52	5.3 GHz	81 kHz	829 kHz
D2	1540	220 MHz	73 MHz	0.5	5.14 GHz	2.56 MHz	1.12 MHz

FIG. 5. Experimental setup for optomechanical spectroscopy. (a) SEM image of the silicon optomechanical crystal cavity. (b) Detailed experimental setup. ECDL, external-cavity diode lasers; FPC, fiber polarization controller; PM, phase modulator; VOA, variable optical attenuator; BHD, balanced heterodyne detector; SA, spectrum analyzer; NA, network analyzer; PLL, phase-locked loop.

in a coherent cavity response. In the incoherent spectroscopy, the reflected light is sent to a balanced heterodyne detection setup by beating with a strong local oscillator, which is phase locked to the blue side of the cooling tone. The photocurrent from the BHD is sent to a spectrum analyzer, enabling a quantum-limited detection of the thermomechanical sideband.

In Fig. 6, the optical cavity resonant wavelength versus the cryostat temperature of a silicon OMC is shown. For temperature above 30 K, $g_{\text{th}} < 0$, with a coefficient
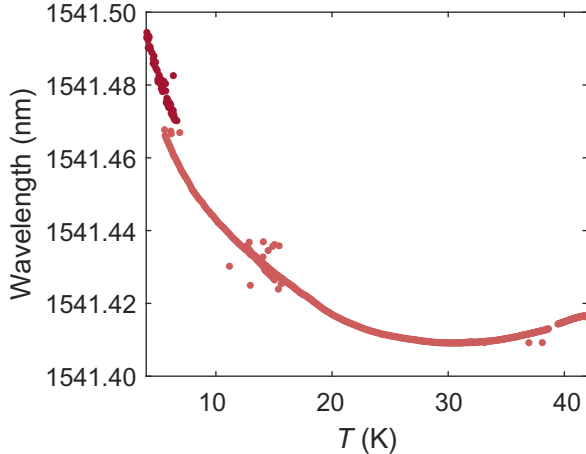

FIG. 6. Optical cavity resonant wavelength versus cryostat temperature of a silicon OMC. The measurement is performed with the OMC with $\kappa/2\pi = 1.6$ GHz at pressure approximately 100 mbar with $\bar{n}_c < 5$ by monitoring the coherent cavity response. The slight color difference at temperature below 8 K corresponds to two different sets of measurements.

a few orders of magnitude lower than room temperature. For temperature below 30 K, $g_{\text{th}} > 0$, as opposed to room temperature. This enables stable strong pumping of the red sideband as required for sideband cooling.

In practice, the absorption rate κ_a differs qualitatively in various fabrication processes and is very difficult to quantify a priori. In principle, κ_a and $\sigma_0(\Omega_m)$ can be jointly fitted from the effective linewidth change [cf. Eq. (14)] and the excess noise floor [cf. Eq. (A10)], as they scale differently with the intracavity photon number. More specifically, we estimate κ_a at room temperature of approximately $2\pi \times 1.5$ MHz, corresponding to $\sigma_0(\Omega)$ of approximately 0.02. We note that, the TPA and FCA in silicon OMC may also result in cavity linewidth increase and frequency blue shift, which is discussed in Appendix D. At cryogenic temperatures (8 K), we estimate $\kappa_a\sigma_0(\Omega_m)$ of $2\pi \times$ 44 kHz. Because of the relatively small noise floor change (1%), we could not reliably quantify the absorption rate of such OMC. We note that, the esimated $\sigma_0(\Omega)$ at room temperature and cryogenic temperature are of the same magnitude while of different sign. As the temperature-dependent cavity frequency shifts (g_{th}) are different by almost 2 orders of magnitude between room temperature and cryogenic temperature, the absorption loss rate κ_a of the OMC at cryogenic temperature may be approximately $2\pi \times 100$ MHz. Such different absorption rates of the two OMCs may explain our previous different optimal ground cooling results, i.e., with final phonon occupancy of 1.5 and 0.1, respectively [31,32].

APPENDIX C: THERMAL RESPONSE SIMULATIONS

In the theoretical treatment of the temperature dynamics in the main text, we neglect the geometric dependence. In practice, the thermal response can be rather complex as dissipative absorption in the microcavities can dissipate via different mechanisms, such as radiation, conduction, and convection. The thermal response can be obtained with finite-element-method (FEM) simulations. We first simulate the electric field distribution of the optical mode $\vec{E}(\vec{r})$. The bulk absorption heating

$$P(\vec{r}) = P_{\text{abs}}\epsilon_0\vec{E}(\vec{r}) \times \hat{\epsilon}\vec{E}(\vec{r})/W_E, \quad (C1)$$

can be added as a heat source in the heat-transfer model, with $\hat{\epsilon} = \hat{\epsilon}_0 + \hat{\epsilon}_1$ the permittivity, and $W_E = \int \epsilon_0\vec{E}(\vec{r}) \times \hat{\epsilon}\vec{E}(\vec{r})dV$ the mode full energy. The frequency component of the temperature distribution $\widetilde{T}(\omega,\vec{r})$ can be solved using the Fourier-domain heat equation,

$$i\Omega\rho C\widetilde{T} + k\Delta\widetilde{T} = \widetilde{P}, \quad (C2)$$

where ρ is the density, C the heat capacity, and k the thermal conductivity. The cavity shift frequency takes the
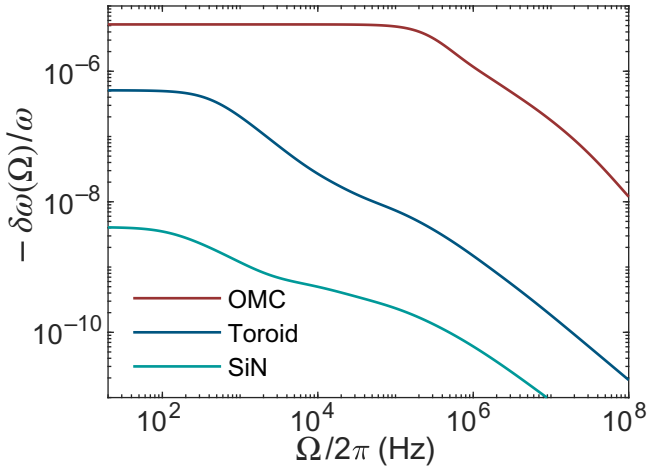
FIG. 7. Simulated cavity frequency response of different microcavities from finite-element simulations at room temperature, including a silicon OMC [30], silica microtoroid [72], and SiN ring resonator [8]. The detailed parameters in the FEM simulation are listed in Table II.

form,

$$\frac{\delta\omega_c(\Omega)}{\omega_c} = -\frac{1}{W_E} \int \widetilde{T}(\Omega, \vec{r}) \epsilon_0 \sqrt{\epsilon(\vec{r})} \frac{dn}{dT}(\vec{r}) |\vec{E}(\vec{r})|^2 dV. \tag{C3}$$

In Fig. 7, we show the cavity frequency responses of three different microcavities, i.e., silicon OMC, silica microtoroid and Si_3N_4 ring resonator, at room temperature with an absorption power $\tilde{P}(\Omega) = 1 \mu W$. The cavity frequency responses deviate from the single-pole model that we use in the main text. Multiple-pole models are typically required to fit the response [31]. The OMC has much larger relative frequency shift at dc compared to the other two types of cavities, due to the small mode volume, which also results in high-frequency poles in MHz range. In microtoroid, despite the large size, the thermal bandwidth can be up to MHz, e.g., in Ref. [97]. For Si_3N_4 microresonator, the bandwidth is typically in the kHz range, e.g., in Ref. [86]. The relevant material coefficients used in the FEM simulations are shown in Table II. In addition to the geometric dependence, the device surroundings sometimes can even have a more significant impact on the cavity frequency thermal response, e.g., gaseous helium, vacuum, or liquid [31,97].

APPENDIX D: EXCESS NOISE

Excess laser noise is known to limit sideband cooling and to introduce classical correlations in linear interferometric measurements of mechanical motion, which becomes extremely critical to deep sideband cooling, where optical filters are typically required to reject the excess laser noise around the mechanical frequency. External cavity diode lasers are well known to have excess noise in the GHz range [26], due to the damped relaxation oscillation caused by carrier population dynamics. In our experiments, the excess laser frequency noise spectrum density $S_\omega(\Omega)$ at a frequency of 5.2 GHz is measured below 10^5 rad^2 Hz. In BHD, we choose a LO power of around 6 mW. The beating between the high reflected power ($> 100 \mu W$) and the noise from the LO can lead to an increased noise floor by approximately 1%, due to the excess noise in the LO [32,98].

Brillouin scattering in optical fibers is known to generate excess noises, from bulk elastic waves or surface acoustic waves [99]. In our experiments, we do not observe evident excess noise in all the optical equipments, such as optical switches, mirrors and fibers, with a quantum-limited detection-balanced heterodyne detection.

Fundamental temperature fluctuation can in principle result in excess thermo-refractive noise (TRN) in the cavity. TRN has received significant attention in the gravitational-wave detection community due to the high powers and low detection bandwidth and limits the ultimate sensitivity. In recent years, there have been continuous efforts in the characterization of TNR in integrated devices. The TRN is estimated to have a large impact on the on-chip Kerr squeezing due to the low detection bandwidth. In our measurements with optomechanical spectroscopy, such effects from TRN might be negligible due to the large mechanical frequency.

The optical resonant wavelength of the silicon OMC is in the band gap of silicon, which should in principle introduce negligible optical absorption. Due to the ultra-small mode volume (approximately λ^3) and the strong cavity field enhancement, nonlinear optical dynamics can arise in the cavity at high pumping powers, such as TPA [82]. The TPA in the silicon cavity can introduce excess nonlinear optical loss κ_{TPA} and generate free carriers. The generated free carriers in turn lead to excess optical loss κ_{FC} and cavity dispersion Δ_{FC}. The total optical cavity loss is thus given by $\kappa = \kappa_{ex} + \kappa_s + \kappa_a + \kappa_{TPA} + \kappa_{FC}$, where $\kappa_{TPA} = \kappa_{TPA}^0 \bar{n}_c$ and $\kappa_{FC} \simeq \kappa_{FC}^0 \bar{n}_c^2$. At room temperature, the estimated $\kappa_{TPA}^0/2\pi \sim 3$ kHz and $\kappa_{FC}^0/2\pi < 10$Hz, taking the parameters in Ref. [82,100,101] and estimated mode volume from finite-element simulation. We note that, κ_{FC}^0

TABLE II. Physical properties used for the FEM simulations of the cavity frequency thermal responses.

Physical properties	Si_3N_4	Si	SiO_2
Density ρ (kg m^{-3})	3290	2329	2203
Refractive index n_0	2.00	3.48	1.50
Thermo-optic dn/dT (10^{-5} K^{-1})	2.45	16.0	1.29
Thermal conductivity k (W m^{-1} K^{-1})	30	130	1.38
Specific heat capacity C (J kg^{-1} K^{-1})	800	700	703

also depends on the carrier lifetime. In our estimation, we assume a carrier lifetime of approximately 10 ns, which in practice depends on the density of the carrier in the optical cavity [82]. At cryogenic temperatures, the carrier lifetime can decrease by a few orders of magnitude compared to room temperature [100], which results in lower κ^0_{FC}. The estimated optical cavity dispersion due to the free carrier by single intracavity photon is $\Delta^0_{FC} < 10$ Hz [82,100,101]. The nonlinear dynamics due to TPA and FC can in principle also result in complex dissipative dynamics in the optical cavity, which is not considered in the main text.

We note that, theoretical predictions show that the free-carrier dispersion in the optical cavity can introduce excess noise due to the incoherent carrier excitation and decay processes [83], which may partially explain the noise floor we observe in the experiments and requires further investigation.

[1] K. J. Vahala, Optical microcavities, Nature **424**, 839 (2003).

[2] A. L. Gaeta, M. Lipson, and T. J. Kippenberg, Photonic-chip-based frequency combs, Nat. Photonics **13**, 158 (2019).

[3] P. Lodahl, S. Mahmoodian, and S. Stobbe, Interfacing single photons and single quantum dots with photonic nanostructures, Rev. Mod. Phys. **87**, 347 (2015).

[4] M. Aspelmeyer, T. J. Kippenberg, and F. Marquardt, Cavity optomechanics, Rev. Mod. Phys. **86**, 1391 (2014).

[5] Y. Akahane, T. Asano, B.-S. Song, and S. Noda, High-Q photonic nanocavity in a two-dimensional photonic crystal, Nature **425**, 944 (2003).

[6] D. K. Armani, T. J. Kippenberg, S. M. Spillane, and K. J. Vahala, Ultra-high-Q toroid microcavity on a chip, Nature **421**, 925 (2003).

[7] M. J. Burek, Y. Chu, M. S. Z. Liddy, P. Patel, J. Rochman, S. Meesala, W. Hong, Q. Quan, M. D. Lukin, and M. Loncar, High quality-factor optical nanocavities in bulk single-crystal diamond, Nat. Commun. **5**, 5718 (2014).

[8] J. Liu, G. Huang, R. N. Wang, J. He, A. S. Raja, T. Liu, N. J. Engelsen, and T. J. Kippenberg, High-yield, wafer-scale fabrication of ultralow-loss, dispersion-engineered silicon nitride photonic circuits, Nat. Commun. **12**, 2236 (2021).

[9] T. Carmon, L. Yang, and K. J. Vahala, Dynamical thermal behavior and thermal self-stability of microcavities, Opt. Express **12**, 4742 (2004).

[10] V. R. Almeida and M. Lipson, Optical bistability on a silicon chip, Opt. Lett. **29**, 2387 (2004).

[11] K. Nozaki, T. Tanabe, A. Shinya, S. Matsuo, T. Sato, H. Taniyama, and M. Notomi, Sub-femtojoule all-optical switching using a photonic-crystal nanocavity, Nat. Photonics **4**, 477 (2010).

[12] F. C. Favero, L. Araujo, G. Bouwmans, V. Finazzi, J. Villatoro, and V. Pruneri, Spheroidal Fabry-Perot microcavities in optical fibers for high-sensitivity sensing, Opt. Express **20**, 7112 (2012).

[13] K. D. Heylman, N. Thakkar, E. H. Horak, S. C. Quillin, C. Cherqui, K. A. Knapper, D. J. Masiello, and R. H. Goldsmith, Optical microresonators as single-particle absorption spectrometers, Nat. Photonics **10**, 788 (2016).

[14] V. B. Braginsky, M. L. Gorodetsky, and S. P. Vyatchanin, Thermodynamical fluctuations and photo-thermal shot noise in gravitational wave antennae, Phys. Lett. A **264**, 1 (1999).

[15] K. Goda, K. McKenzie, E. E. Mikhailov, P. K. Lam, D. E. McClelland, and N. Mavalvala, Photothermal fluctuations as a fundamental limit to low-frequency squeezing in a degenerate optical parametric oscillator, Phys. Rev. A **72**, 043819 (2005).

[16] A. B. Matsko, A. A. Savchenkov, N. Yu, and L. Maleki, Whispering-gallery-mode resonators as frequency references I fundamental limitations, J. Opt. Soc. Am. B **24**, 1324 (2007).

[17] X. Sun, R. Luo, X.-C. Zhang, and Q. Lin, Squeezing the fundamental temperature fluctuations of a high-Q microresonator, Phys. Rev. A **95**, 023822 (2017).

[18] T. E. Drake, J. R. Stone, T. C. Briles, and S. B. Papp, Thermal decoherence and laser cooling of Kerr microresonator solitons, Nat. Photonics **14**, 480 (2020).

[19] S. De Liberato, N. Lambert, and F. Nori, Quantum noise in photothermal cooling, Phys. Rev. A **83**, 033809 (2011).

[20] J. Restrepo, J. Gabelli, C. Ciuti, and I. Favero, Classical and quantum theory of photothermal cavity cooling of a mechanical oscillator, Comptes Rendus Physique Nano-and Micro-Optomechanical Systems **12**, 860 (2011).

[21] J. R. Stone, T. C. Briles, T. E. Drake, D. T. Spencer, D. R. Carlson, S. A. Diddams, and S. B. Papp, Thermal and Nonlinear Dissipative-Soliton Dynamics in Kerr-Microresonator Frequency Combs, Phys. Rev. Lett. **121**, 063902 (2018).

[22] J. H. Shapiro, G. Saplakoglu, S.-T. Ho, P. Kumar, B. E. A. Saleh, and M. C. Teich, Theory of light detection in the presence of feedback, JOSA B **4**, 1604 (1987).

[23] M. S. Taubman, H. Wiseman, D. E. McClelland, and H.-A. Bachor, Intensity feedback effects on quantum-limited noise, J. Opt. Soc. Am. B **12**, 1792 (1995).

[24] H. M. Wiseman, Squashed states of light: Theory and applications to quantum spectroscopy, J. Opt. B: Quantum Semiclassical Opt. **1**, 459 (1999).

[25] H. M. Wiseman, In-Loop Squeezing Is Like Real Squeezing to an In-Loop Atom, Phys. Rev. Lett. **81**, 3840 (1998).

[26] T. J. Kippenberg, A. Schliesser, and M. L. Gorodetsky, Phase noise measurement of external cavity diode lasers and implications for optomechanical sideband cooling of GHz mechanical modes, New J. Phys. **15**, 015019 (2013).

[27] P. Rabl, C. Genes, K. Hammerer, and M. Aspelmeyer, Phase-noise induced limitations on cooling and coherent evolution in optomechanical systems, Phys. Rev. A **80**, 063819 (2009).

[28] A. H. Safavi-Naeini, J. Chan, J. T. Hill, S. Gröblacher, H. Miao, Y. Chen, M. Aspelmeyer, and O. Painter, Laser noise in cavity-optomechanical cooling and thermometry, New J. Phys. **15**, 035007 (2013).

[29] M. Eichenfield, J. Chan, R. M. Camacho, K. J. Vahala, and O. Painter, Optomechanical crystals, Nature **462**, 78 (2009).

[30] J. Chan, A. H. Safavi-Naeini, J. T. Hill, S. Meenehan, and O. Painter, Optimized optomechanical crystal cavity with acoustic radiation shield, Appl. Phys. Lett. **101**, 081115 (2012).

[31] L. Qiu, I. Shomroni, M. A. Ioannou, N. Piro, D. Malz, A. Nunnenkamp, and T. J. Kippenberg, Floquet dynamics in the quantum measurement of mechanical motion, Phys. Rev. A **100**, 053852 (2019).

[32] L. Qiu, I. Shomroni, P. Seidler, and T. J. Kippenberg, Laser Cooling of a Nanomechanical Oscillator to Its Zero-Point Energy, Phys. Rev. Lett. **124**, 173601 (2020).

[33] I. Shomroni, L. Qiu, D. Malz, A. Nunnenkamp, and T. J. Kippenberg, Optical backaction-evading measurement of a mechanical oscillator, Nat. Commun. **10**, 2086 (2019).

[34] I. Shomroni, A. Youssefi, N. Sauerwein, L. Qiu, P. Seidler, D. Malz, A. Nunnenkamp, and T. J. Kippenberg, Two-Tone Optomechanical Instability and Its Fundamental Implications for Backaction-Evading Measurements, Phys. Rev. X **9**, 041022 (2019).

[35] I. Wilson-Rae, N. Nooshi, W. Zwerger, and T. J. Kippenberg, Theory of Ground State Cooling of a Mechanical Oscillator Using Dynamical Backaction, Phys. Rev. Lett. **99**, 093901 (2007).

[36] F. Marquardt, J. P. Chen, A. A. Clerk, and S. M. Girvin, Quantum Theory of Cavity-Assisted Sideband Cooling of Mechanical Motion, Phys. Rev. Lett. **99**, 093902 (2007).

[37] J. Chan, T. P. Alegre, A. H. Safavi-Naeini, J. T. Hill, A. Krause, S. Gröblacher, M. Aspelmeyer, and O. Painter, Laser cooling of a nanomechanical oscillator into its quantum ground state, Nature **478**, 89 (2011).

[38] J. D. Teufel, T. Donner, D. Li, J. W. Harlow, M. S. Allman, K. Cicak, A. J. Sirois, J. D. Whittaker, K. W. Lehnert, and R. W. Simmonds, Sideband cooling of micromechanical motion to the quantum ground state, Nature **475**, 359 (2011).

[39] D. J. Wilson, V. Sudhir, N. Piro, R. Schilling, A. Ghadimi, and T. J. Kippenberg, Measurement-based control of a mechanical oscillator at its thermal decoherence rate, Nature **524**, 325 (2015).

[40] M. Rossi, D. Mason, J. Chen, Y. Tsaturyan, and A. Schliesser, Measurement-based quantum control of mechanical motion, Nature **563**, 53 (2018).

[41] N. Aggarwal, T. J. Cullen, J. Cripe, G. D. Cole, R. Lanza, A. Libson, D. Follman, P. Heu, T. Corbitt, and N. Mavalvala, Room-temperature optomechanical squeezing, Nat. Phys. **16**, 784 (2020).

[42] N. S. Kampel, R. W. Peterson, R. Fischer, P. L. Yu, K. Cicak, R. W. Simmonds, K. W. Lehnert, and C. A. Regal, Improving Broadband Displacement Detection with Quantum Correlations, Phys. Rev. X **7**, 021008 (2017).

[43] T. P. Purdy, P. L. Yu, R. W. Peterson, N. S. Kampel, and C. A. Regal, Strong Optomechanical Squeezing of Light, Phys. Rev. X **3**, 031012 (2013).

[44] A. H. Safavi-Naeini, S. Gröblacher, J. T. Hill, J. Chan, M. Aspelmeyer, and O. Painter, Squeezed light from a silicon micromechanical resonator, Nature **500**, 185 (2013).

[45] V. Sudhir, R. Schilling, S. A. Fedorov, H. Schütz, D. J. Wilson, and T. J. Kippenberg, Quantum Correlations of

Light from a Room-Temperature Mechanical Oscillator, Phys. Rev. X **7**, 031055 (2017).

[46] A. H. Safavi-Naeini, J. Chan, J. T. Hill, T. P. Alegre, A. Krause, and O. Painter, Observation of Quantum Motion of a Nanomechanical Resonator, Phys. Rev. Lett. **108**, 033602 (2012).

[47] A. J. Weinstein, C. U. Lei, E. E. Wollman, J. Suh, A. Metelmann, A. A. Clerk, and K. C. Schwab, Observation and Interpretation of Motional Sideband Asymmetry in a Quantum Electromechanical Device, Phys. Rev. X **4**, 041003 (2014).

[48] V. Sudhir, D. J. Wilson, R. Schilling, H. Schütz, S. A. Fedorov, A. H. Ghadimi, A. Nunnenkamp, and T. J. Kippenberg, Appearance and Disappearance of Quantum Correlations in Measurement-Based Feedback Control of a Mechanical Oscillator, Phys. Rev. X **7**, 011001 (2017).

[49] N. R. Bernier, L. D. Tóth, A. Koottandavida, M. A. Ioannou, D. Malz, A. Nunnenkamp, A. K. Feofanov, and T. J. Kippenberg, Nonreciprocal reconfigurable microwave optomechanical circuit, Nat. Commun. **8**, 604 (2017).

[50] G. A. Peterson, F. Lecocq, K. Cicak, R. W. Simmonds, J. Aumentado, and J. D. Teufel, Demonstration of Efficient Nonreciprocity in a Microwave Optomechanical Circuit, Phys. Rev. X **7**, 031001 (2017).

[51] H. Xu, L. Jiang, A. A. Clerk, and J. G. E. Harris, Nonreciprocal control and cooling of phonon modes in an optomechanical system, Nature **568**, 65 (2019).

[52] J. T. Hill, A. H. Safavi-Naeini, J. Chan, and O. Painter, Coherent optical wavelength conversion via cavity optomechanics, Nat. Commun. **3**, 1196 (2012).

[53] G. Arnold, M. Wulf, S. Barzanjeh, E. S. Redchenko, A. Rueda, W. J. Hease, F. Hassani, and J. M. Fink, Converting microwave and telecom photons with a silicon photonic nanomechanical interface, Nat. Commun. **11**, 4460 (2020).

[54] J. Bochmann, A. Vainsencher, D. D. Awschalom, and A. N. Cleland, Nanomechanical coupling between microwave and optical photons, Nat. Phys. **9**, 712 (2013).

[55] A. P. Higginbotham, P. S. Burns, M. D. Urmey, R. W. Peterson, N. S. Kampel, B. M. Brubaker, G. Smith, K. W. Lehnert, and C. A. Regal, Harnessing electro-optic correlations in an efficient mechanical converter, Nat. Phys. **14**, 1038 (2018).

[56] W. Jiang, C. J. Sarabalis, Y. D. Dahmani, R. N. Patel, F. M. Mayor, T. P. McKenna, R. Van Laer, and A. H. Safavi-Naeini, Efficient bidirectional piezo-optomechanical transduction between microwave and optical frequency, Nat. Commun. **11**, 1166 (2020).

[57] M. Mirhosseini, A. Sipahigil, M. Kalaee, and O. Painter, Superconducting qubit to optical photon transduction, Nature **588**, 599 (2020).

[58] M. Wu, E. Zeuthen, K. C. Balram, and K. Srinivasan, Microwave-To-Optical Transduction Using a Mechanical Supermode for Coupling Piezoelectric and Optomechanical Resonators, Phys. Rev. Appl. **13**, 014027 (2020).

[59] S. Hong, R. Riedinger, I. Marinković, A. Wallucks, S. G. Hofer, R. A. Norte, M. Aspelmeyer, and S. Gröblacher, Hanbury Brown and Twiss interferometry of single phonons from an optomechanical resonator, Science **358**, 203 (2017).

[60] I. Marinković, A. Wallucks, R. Riedinger, S. Hong, M. Aspelmeyer, and S. Gröblacher, Optomechanical Bell Test, Phys. Rev. Lett. **121**, 220404 (2018).

[61] C. F. Ockeloen-Korppi, E. Damskägg, J. M. Pirkkalainen, M. Asjad, A. A. Clerk, F. Massel, M. J. Woolley, and M. A. Sillanpää, Stabilized entanglement of massive mechanical oscillators, Nature **556**, 478 (2018).

[62] R. Riedinger, A. Wallucks, I. Marinković, C. Löschnauer, M. Aspelmeyer, S. Hong, and S. Gröblacher, Remote quantum entanglement between two micromechanical oscillators, Nature **556**, 473 (2018).

[63] I. Shomroni, L. Qiu, and T. J. Kippenberg, Optomechanical generation of a mechanical catlike state by phonon subtraction, Phys. Rev. A **101**, 033812 (2020).

[64] A. Kronwald, F. Marquardt, and A. A. Clerk, Arbitrarily large steady-state bosonic squeezing via dissipation, Phys. Rev. A - At., Mol., Opt. Phys. **88**, 063833 (2013).

[65] F. Lecocq, J. B. Clark, R. W. Simmonds, J. Aumentado, and J. D. Teufel, Quantum Nondemolition Measurement of a Nonclassical State of a Massive Object, Phys. Rev. X **5**, 041037 (2015).

[66] J. M. Pirkkalainen, E. Damskägg, M. Brandt, F. Massel, and M. A. Sillanpää, Squeezing of Quantum Noise of Motion in a Micromechanical Resonator, Phys. Rev. Lett. **115**, 243601 (2015).

[67] E. E. Wollman, C. U. Lei, A. J. Weinstein, J. Suh, A. Kronwald, F. Marquardt, A. A. Clerk, and K. C. Schwab, Quantum squeezing of motion in a mechanical resonator, Science **349**, 952 (2015).

[68] T. P. Purdy, P. L. Yu, N. S. Kampel, R. W. Peterson, K. Cicak, R. W. Simmonds, and C. A. Regal, Optomechanical Raman-ratio thermometry, Phys. Rev. A - At., Mol., Opt. Phys. **92**, 031802 (2015).

[69] M. Underwood, D. Mason, D. Lee, H. Xu, L. Jiang, A. B. Shkarin, K. Børkje, S. M. Girvin, and J. G. Harris, Measurement of the motional sidebands of a nanogram-scale oscillator in the quantum regime, Phys. Rev. A - At., Mol., Opt. Phys. **92**, 061801 (2015).

[70] R. W. Peterson, T. P. Purdy, N. S. Kampel, R. W. Andrews, P.-L. Yu, K. W. Lehnert, and C. A. Regal, Laser Cooling of a Micromechanical Membrane to the Quantum Backaction Limit, Phys. Rev. Lett. **116**, 063601 (2016).

[71] Y. Tsaturyan, A. Barg, E. S. Polzik, and A. Schliesser, Ultracoherent nanomechanical resonators via soft clamping and dissipation dilution, Nat. Nanotechnol. **12**, 776 (2017).

[72] E. Verhagen, S. Deléglise, S. Weis, A. Schliesser, and T. J. Kippenberg, Quantum-coherent coupling of a mechanical oscillator to an optical cavity mode, Nature **482**, 63 (2012).

[73] M. Rossi, N. Kralj, S. Zippilli, R. Natali, A. Borrielli, G. Pandraud, E. Serra, G. Di Giuseppe, and D. Vitali, Enhancing Sideband Cooling by Feedback-Controlled Light, Phys. Rev. Lett. **119**, 123603 (2017).

[74] M. Rossi, N. Kralj, S. Zippilli, R. Natali, A. Borrielli, G. Pandraud, E. Serra, G. Di Giuseppe, and D. Vitali, Normal-Mode Splitting in a Weakly Coupled Optomechanical System, Phys. Rev. Lett. **120**, 073601 (2018).

[75] S. Zippilli, N. Kralj, M. Rossi, G. Di Giuseppe, and D. Vitali, Cavity optomechanics with feedback-controlled in-loop light, Phys. Rev. A **98**, 023828 (2018).

[76] H. A. Haus and Y. Yamamoto, Theory of feedback-generated squeezed states, Phys. Rev. A **34**, 270 (1986).

[77] C. W. Gardiner and M. J. Collett, Input and output in damped quantum systems: Quantum stochastic differential equations and the master equation, Phys. Rev. A **31**, 3761 (1985).

[78] A. H. Safavi-Naeini, T. P. M. Alegre, J. Chan, M. Eichenfield, M. Winger, Q. Lin, J. T. Hill, D. E. Chang, and O. Painter, Electromagnetically induced transparency and slow light with optomechanics, Nature **472**, 69 (2011).

[79] S. Weis, R. Rivière, S. Deléglise, E. Gavartin, O. Arcizet, A. Schliesser, and T. J. Kippenberg, Optomechanically induced transparency, Science **330**, 1520 (2010).

[80] C. H. Metzger and K. Karrai, Cavity cooling of a microlever, Nature **432**, 1002 (2004).

[81] J. Ma, J. Qin, G. T. Campbell, R. Lecamwasam, K. Sripathy, J. Hope, B. C. Buchler, and P. K. Lam, Photothermally induced transparency, Sci. Adv. **6**, 8256 (2020).

[82] P. E. Barclay, K. Srinivasan, and O. Painter, Nonlinear response of silicon photonic crystal microresonators excited via an integrated waveguide and fiber taper, Opt. Express **13**, 801 (2005).

[83] R. Hamerly and H. Mabuchi, Quantum noise of free-carrier dispersion in semiconductor optical cavities, Phys. Rev. A **92**, 023819 (2015).

[84] A. B. Matsko, A. A. Savchenkov, D. Strekalov, V. S. Ilchenko, and L. Maleki, Optical hyperparametric oscillations in a whispering-gallery-mode resonator: Threshold and phase diffusion, Phys. Rev. A **71**, 033804 (2005).

[85] V. B. Braginsky, M. L. Gorodetsky, and S. P. Vyatchanin, Thermo-refractive noise in gravitational wave antennae, Phys. Lett. A **271**, 303 (2000).

[86] G. Huang, E. Lucas, J. Liu, A. S. Raja, G. Lihachev, M. L. Gorodetsky, N. J. Engelsen, and T. J. Kippenberg, Thermorefractive noise in silicon-nitride microresonators, Phys. Rev. A **99**, 061801 (2019).

[87] C. Panuski, D. Englund, and R. Hamerly, Fundamental Thermal Noise Limits for Optical Microcavities, Phys. Rev. X **10**, 041046 (2020).

[88] M. Li, H. Liang, R. Luo, Y. He, J. Ling, and Q. Lin, Photon-level tuning of photonic nanocavities, Optica **6**, 860 (2019).

[89] R. Sahu, W. Hease, A. Rueda, G. Arnold, L. Qiu, and J. Fink, Quantum-enabled interface between microwave and telecom light, (2021), ArXiv:2107.08303.

[90] J. Holzgrafe, N. Sinclair, N. Sinclair, D. Zhu, D. Zhu, A. Shams-Ansari, M. Colangelo, Y. Hu, Y. Hu, M. Zhang, M. Zhang, K. K. Berggren, and M. Lončar, Cavity electro-optics in thin-film lithium niobate for efficient microwave-to-optical transduction, Optica **7**, 1714 (2020).

[91] A. Blais, A. L. Grimsmo, S. M. Girvin, and A. Wallraff, Circuit quantum electrodynamics, Rev. Mod. Phys. **93**, 025005 (2021).

[92] I. M. Pop, K. Geerlings, G. Catelani, R. J. Schoelkopf, L. I. Glazman, and M. H. Devoret, Coherent suppression of electromagnetic dissipation due to superconducting quasiparticles, Nature **508**, 369 (2014).

[93] A. Bespalov, M. Houzet, J. S. Meyer, and Y. V. Nazarov, Theoretical Model to Explain Excess of Quasiparticles in Superconductors, Phys. Rev. Lett. **117**, 117002 (2016).

[94] S. Gustavsson, F. Yan, G. Catelani, J. Bylander, A. Kamal, J. Birenbaum, D. Hover, D. Rosenberg, G. Samach, A. P. Sears, S. J. Weber, J. L. Yoder, J. Clarke, A. J. Kerman, F. Yoshihara, Y. Nakamura, T. P. Orlando, and W. D. Oliver, Suppressing relaxation in superconducting qubits by quasiparticle pumping, Science **354**, 1573 (2016).

[95] T. Tai, J. Cai, and S. M. Anlage, Coherence Time Enhancement of Interacting Two-Level Systems in Aluminum Superconducting Resonators, (2021), ArXiv:2109.11742.

[96] L. Qiu, G. Huang, I. Shomroni, J. Pan, P. Seidler, and T. J. Kippenberg, Data for: "Dissipative quantum feedback in measurements using a parametrically coupled microcavity," https://doi.org/10.5281/zenodo.6364804 (2022).

[97] R. Rivière, *Cavity Optomechanics with Silica Toroidal Microresonators down to Low Phonon Occupancy*, Phd, school Ludwig-Maximilians-Universität, Munchen2011.

[98] L. Qiu, *Quantum Measurement of Mechanical Motion Close to the Standard Quantum Limit*, Phd, school Swiss Federal Institute of Technology in Lausanne (EPFL), Lausanne2020.

[99] J.-C. Beugnot, S. Lebrun, G. Pauliat, H. Maillotte, V. Laude, and T. Sylvestre, Brillouin light scattering from surface acoustic waves in a subwavelength-diameter optical fibre, Nat. Commun. **5**, 5242 (2014).

[100] X. Sun, X. Zhang, C. Schuck, and H. X. Tang, Nonlinear optical effects of ultrahigh-Q silicon photonic nanocavities immersed in superfluid helium, Sci. Rep. **3**, 1436 (2013).

[101] J. Wu, S.-W. Huang, Y. Huang, H. Zhou, J. Yang, J.-M. Liu, M. Yu, G. Lo, D.-L. Kwong, S. Duan, and C. Wei Wong, Mesoscopic chaos mediated by Drude electron-hole plasma in silicon optomechanical oscillators, Nat. Commun. **8**, 15570 (2017).